Can the Binuclear Dinitrogen Complex $[P_2N_2]Zr(\mu\text{-}\eta^2\text{-}N_2)Zr[P_2N_2]$ Activate More Than One Hydrogen Molecule? A Theoretical Study

Harold Basch,*,† Djamaladdin G. Musaev,*,‡ and Keiji Morokuma*,‡

Cherry L. Emerson Center for Scientific Computation and Department of Chemistry, Emory University, Atlanta, Georgia 30322, and Department of Chemistry, Bar Ilan University, Ramat Gan 52900, Israel

Received May 8, 2000

The reaction mechanisms of model complexes$[p_2n_2]Zr(\mu\text{-}\eta^2\text{-}NNH)(\mu\text{-}H)Zr[p_2n_2]$, **B1 (A7)**, $[p_2n_2](H)Zr(\mu\text{-}\eta^2\text{-}NNH)Zr[p_2n_2]$, **B11 (A3)**, $[p_2n_2]Zr(\mu\text{-}\eta^2\text{-}cis\text{-}HNNH)(\mu\text{-}H)Zr(H)[p_2n_2]$, **C1 (B3)**, $[p_2n_2](H)Zr(\mu\text{-}\eta^2\text{-}cis\text{-}HNNH)Zr(H)[p_2n_2]$, **C4 (B13)**, $[p_2n_2](H)Zr(\mu\text{-}\eta^2\text{-}trans\text{-}HNNH)Zr\ (H)[p_2n_2]$, **C7 (B21)**, where $[p_2n_2] = [(PH_3)(NH_2)]$, with molecular hydrogen have been studied using density functional theory and compared with those for $[p_2n_2]Zr(\mu\text{-}\eta^2\text{-}N_2)Zr[p_2n_2]$, **A1.** The addition of a H_2 molecule to **B1** (**A7**) (i.e., the addition of the second H_2 to **A1**) takes place with a 19.5 kcal/mol barrier, which is about 2 kcal/mol smaller than that for the first H_2 addition **A1** + H_2 → **A7** reaction. From **B3**, product of **B1** + H_2, the process proceeds via either channel **I.a**, the reverse reaction **B3** → **B1** + H_2, or/and channel **I.b**, the dihydrogen elimination **B3** → $[p_2n_2]Zr(\mu\text{-}\eta^2\text{-}cis\text{-}HNNH)Zr[p_2n_2]$ (**A15**) + H_2, with barriers of 11.7 and 21.5 kcal/mol, respectively. Since addition of the first H_2 to **A1** is known to occur at laboratory conditions, one predicts that the addition of the H_2 to **B1** (**A7**) will also be feasible under proper experimental conditions. Once **A15** is produced, reaction leads to $[p_2n_2]Zr(\mu\text{-}NH)(\mu\text{-}NH_2)(\mu\text{-}H)Zr[p_2n_2]$ (**B8**) via formation of $[p_2n_2]Zr(\mu\text{-}NH)_2Zr[p_2n_2]$, **A17,** which was kinetically unreachable by **A1** + H_2 because of a very high barrier separating it from **A7**. Addition of H_2 to the intermediate complex **B11 (A3)** leads to **B13**, where the N−H bonds are located cis to each other. Subsequently, **B13** most likely rearranges to complex **B3** and follows the reactions of **B3**. Addition of the third H_2 molecule to **A1** is found to be kinetically less favorable than the first two.

1. Introduction

Activation and utilization of the dinitrogen molecule has been a focus of research for the past several decades.[1] Extensive studies have led to the discovery of several new and interesting reactions involving the dinitrogen molecule.[2−4] One of these is the reaction of a coordinated dinitrogen molecule with molecular hydrogen. Recently, Fryzuk and co-workers[4] reported experiments where the dihydrogen molecule added to the binuclear metal dinitrogen complex $[P_2N_2]Zr(\mu\text{-}\eta^2\text{−}N_2)\text{-}Zr[P_2N_2]$, **I**, where $[P_2N_2] = PhP(CH_2SiMe_2NSiMe_2\text{-}CH_2)_2PPh$. It was shown that complex **I** containing a coordinated N_2 molecule in the side-on bridging position reacted with the dihydrogen molecule to produce a new complex having bridging Zr···H···Zr and N−H bonds: $[P_2N_2]Zr(\mu\text{-}\eta^2\text{-}N_2H)Zr[P_2N_2](\mu\text{-}H)$, **II**, where the original H−H bond is broken, while the N−N bond is conserved. This represented the first example of the addition of a hydrogen molecule to a metal-coordinated N_2 molecule. The ultimate goal would be to form free ammonia.[4]

Our previous theoretical studies[5,6] of the reaction mechanism of model complex **1**, $[p_2n_2\}Zr(\mu\text{-}\eta^2\text{−}N_2)Zr\text{-}[p_2n_2]$, where $[p_2n_2] = (PH_3)_2(NH_2)_2$, with dihydrogen demonstrated, as shown in Figure 1, that this reaction proceeds in two steps: (i) the activation of the H−H bond through a "metathesis-like" transition state **A2**, where simultaneous Zr−H and N−H bonds are formed and the H−H and one of N−N π-bonds are broken, to produce the diazenidohydride complex, **A3**; (ii) migra-

† Bar Ilan University.
‡ Emory University.

(1) (a) *Catalytic Ammonia Synthesis*; Jennings, J. R., Eds.; Plenum: New York, 1991. (b) Ludden, P. W. *Encyclopedia of Inorganic Chemistry*; Wiley: New York, 1994; p 2566. (c) Coucouvanis, D. *Encyclopedia of Inorganic Chemistry*; Wiley: New York, 1994; p 2557. (d) Howard, J. B.; Rees, D. C. *Chem. Rev.* **1996**, *96*, 2965. (e) Burgess, B. K.; Lowe, D. J. *Chem. Rev.* **1996**, *96*, 2983. (f) Eady, R. R. *Chem. Rev.* **1996**, *96*, 3013. (g) Leigh, G. J., *Science* **1998**, *279*, 506. (h) Leigh, G. J. *Acc. Chem. Res.* **1992**, *25*, 177, and references therein. (i) Eady, R. R. *Perspectives on Bioinorganic Chem.*; JAI Press: Greenwich, CT, 1991; p 255. (j) Kim, J.; Rees, D. C. *Science* **1992**, *257*, 1667. (k) Kim, J.; Rees, D. C. *Nature* **1992**, *360*, 553. (l) Chan, M. K.; Kim, J.; Rees, D. C. *Science* **1993**, *260*, 792. (m) Demadis, K. D.; Coucouvanis, D. *Inorg. Chem.* **1995**, *34*, 436. (n) Malinak, S. M.; Simeonov, A. M.; Mosier, P. E.; McKenna, C. E.; Coucouvanis, D. *J. Am. Chem. Soc.* **1997**, *119*, 1662, and references therein.

(2) (a) Laplaza, C. E.; Cummins, C. C. *Science* **1995**, *268*, 861. (b) Laplaza, C. E.; Odom, A. L.; Davis, W. M.; Cummins, C. C. *J. Am. Chem. Soc.* **1995**, *117*, 4999. (c) Odom, A. L.; Cummins, C. C. *J. Am. Chem. Soc.* **1995**, *117*, 6613. (d) Laplaza, C. E.; Johnson, A. R.; Cummins, C. C. *J. Am. Chem. Soc.* **1996**, *118*, 709. (e) Laplaza, C. E.; Johnson, M. J. A.; Peters, J. C.; Odom, A. L.; Kim, E.; Cummins, C. C.; George, G. N.; Pickering, I. J., *J. Am. Chem. Soc.* **1996**, *118*, 8623.

(3) Nishibayashi, Y.; Iwai, S.; Hidai, M. *Science* **1998**, *279*, 540.

(4) Fryzuk, M. D.; Love, J. B.; Rettig, S. J.; Young, V. G. *Science* **1997**, *275*, 1445.

(5) Basch, H.; Musaev, D. G.; Morokuma, K.; Fryzuk, M. D.; Love, J. B.; Seidel, W. W.; Albinati, A.; Koetzle, T. F.; Klooster, W. T.; Mason, S. A.; Eckert, J. *J. Am. Chem. Soc.* **1999**, *121*, 523.

(6) Basch, H.; Musaev, D. G.; Morokuma, K. *J. Am. Chem. Soc.* **1999**, *121*, 5754.

10.1021/om000389z CCC: $19.00
Publication on Web 07/12/2000

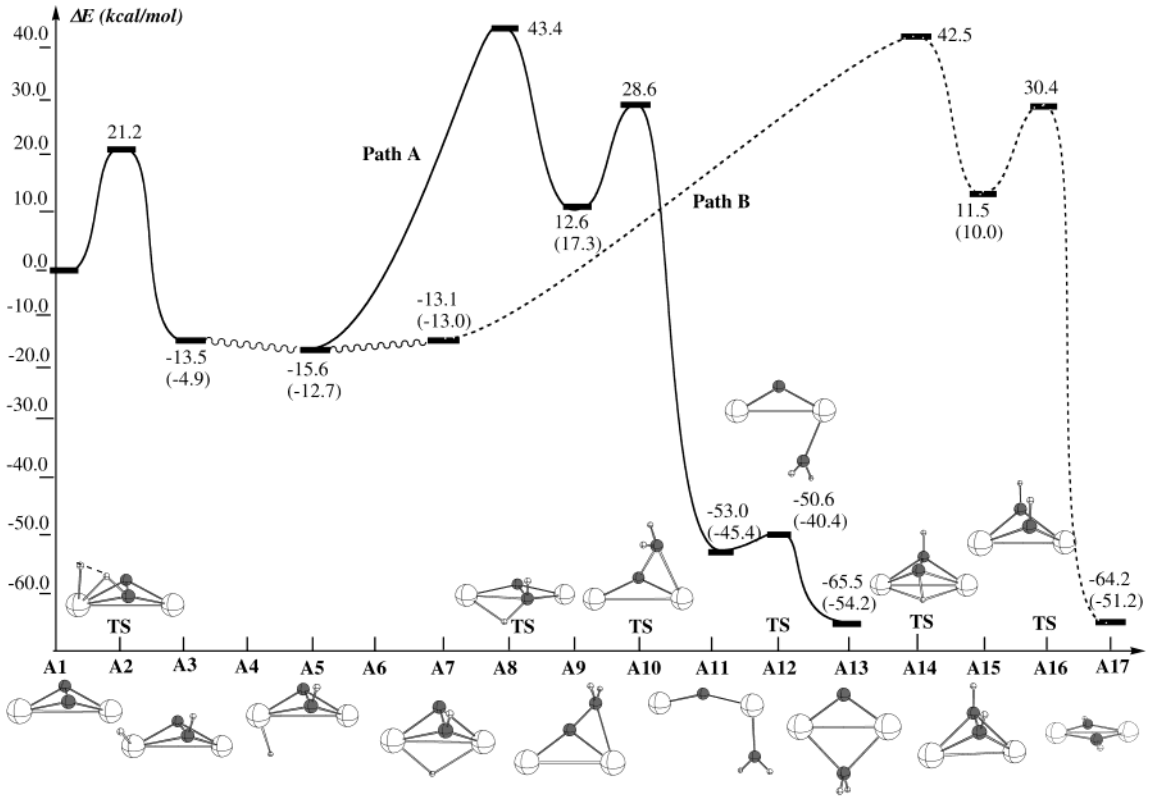

Figure 1. Calculated potential energy profile of the reaction **A1** + H_2.[6] For clarity, the ancillary PH_3 and NH_2 ligands are omitted in the illustration. Numbers given in parentheses were obtained upon constraining the Zr−P bond distances at 2.80 Å.

tion of the Zr-bonded hydride ligand to a position bridging the two Zr atoms to form the diazenido-μ-hydride complex, **A7**. The entire reaction is calculated to be exothermic by 13−15 kcal/mol. The rate-determining step of the reaction is found to be the H−H bond activation step, which occurs with a 21 kcal/mol barrier. We should note that the diazenido-μ-hydride complex, **A7**, experimentally observed in solution, is not the lowest energy structure on the reaction path. Both the hydrazono complex **A13** with a bridging NH_2 and the hydrado complex **A17** with two bridging NH units are calculated to be more stable than **A7** by about 40−50 kcal/mol. However, these former complexes cannot be generated by the reaction of **A1** + H_2 at ambient conditions because of very high (nearly 55−60 kcal/mol) barriers at **A10** and **A14** separating them from **A7**. Experimentally,[4] only **A7** is found; presumably because it is a few kcal/mol more stable than **A3** or **A5** in the Zr−P constrained calculations.

These previous studies showed that only one Zr and one N center are used in the initial reaction with H_2; one H atom is bound to the N_2 molecule, and the second H atom is "wasted" by forming a bond with Zr. The other N and Zr centers seem to be still available for a second H−H bond activation process. Therefore, the question can be asked whether the addition of a second molecule of H_2 would be feasible.

The present paper studies the feasibility of adding a second molecule hydrogen to the previously derived systems**.** The complexes that can serve as initial reactants for a second H_2 addition reaction are **A3** and **A7** described above, which are located "before" the higher barrier walls that connect to **A13** and **A17**. We have therefore carried out a computational experiment using the same DFT method as in the previous studies to explore the reaction paths for the **A3** + H_2 and **A7** + H_2 reactions.

To anticipate the results, we did find that a second H_2 addition gives initial products that are stable and have barrier heights similar to that of the first H_2 addition. We, therefore, continued the computational experiment with the addition of a third molecule of H_2, starting from the intermediates of the second H_2 activation. The aim of these studies is to suggest reactions that could eventually lead to the release of NH_3 or related processes. We use labels **B** and **C** to distinguish the intermediates and transition states of the second and third H_2 addition processes, respectively, from the **A** structures of the first H_2 addition.

2. Computational Procedure

As described previously,[5,6] the model complex chosen to represent structure **I** of the experimental system has the form $[p_2n_2]Zr(\mu\text{-}\eta^2\text{-}N_2)Zr[p_2n_2]$, where $[p_2n_2] = (PH_3)(NH_2)$. Thus, the coordinated phosphines and nitrogens of the tetradentate macrocyclic $[P_2N_2]$ ligand on each Zr atom are preserved, while H atoms replace two CH_2 and a phenyl group on each phosphorus and two $SiMe_2$ groups on each nitrogen. Since the coordinating P and N atoms are not connected in the model as in the actual macrocyclic ligand, the structurally rigid aspect of the extended ligand is lost. In addition, the electronic and steric effect of the phenyl groups is absent in the model phosphine ligands.

The simplification of using $[p_2n_2] = [(PH_3)(NH_2)]$ in the model complexes instead of the real macrocyclic $[P_2N_2]$ ligand resulted in a weaker Zr−P bond.[6] The rigid macrocyclic

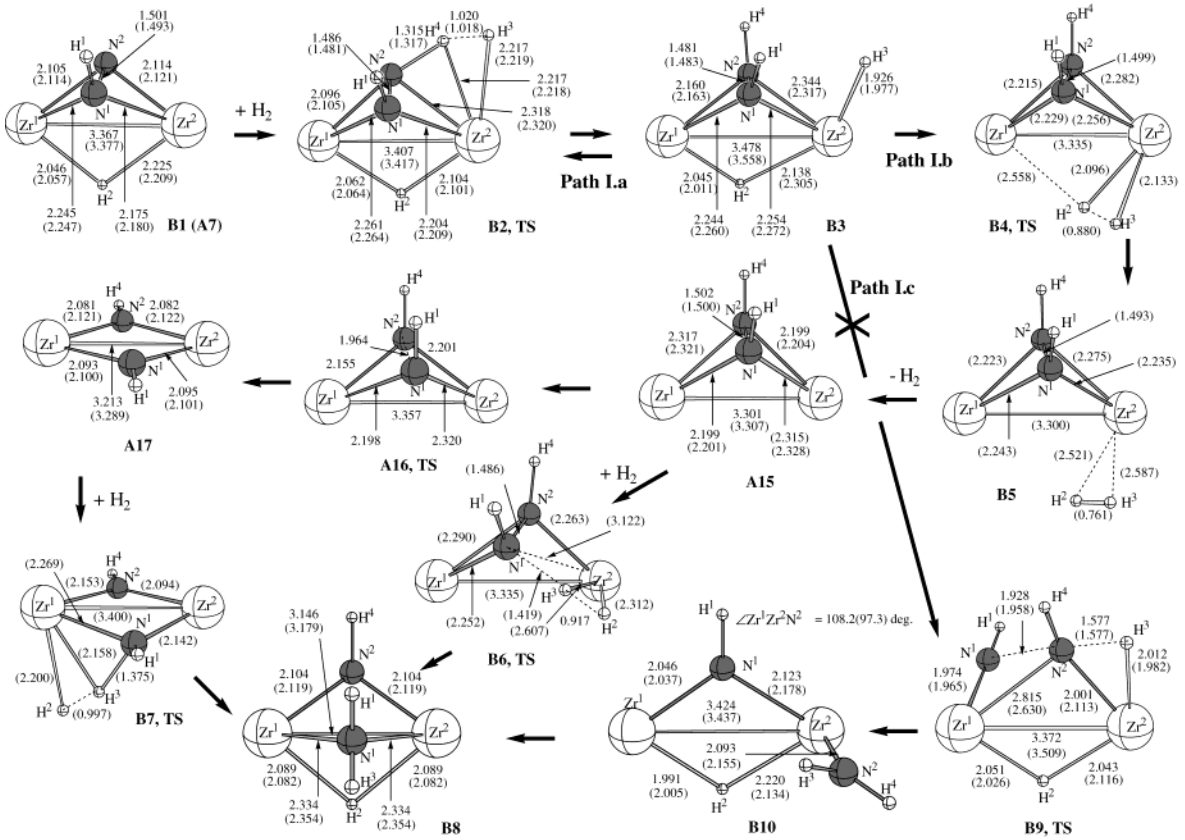

Figure 2. The calculated geometries (distances in Å, angles in deg) of the reactants, intermediates, transition states, and products of the reaction **B1 (A7)** + H_2. For clarity, the ancillary PH_3 and NH_2 ligands are omitted. Numbers given in parentheses were obtained upon constraining the Zr−P bond distances at 2.80 Å (see text for details).

structure of the $[P_2N_2]$ complexes, with the strong Zr−N bonds, will prevent an excessive lengthening of the Zr−P bond distance. In our calculations on the model complex, we found that the Zr−PH_3 distances were larger by ∼0.2 Å compared to experiment for **I**. In this study the strength of the Zr−P bond and its effect on the calculated Zr−P distances and the energetics of the reactions were handled in the same way as was done in our earlier paper,[6] by also optimizing all equilibrium geometries using a fixed Zr−P bond distance of 2.80 Å to simulate the constraints of the macrocyclic ligand. These results will be discussed and interpreted alongside the unconstrained results. In the future, the effects of substituents on the coordinated PH_3 (and NH_2) groups will be more accurately described by the IMOMM and IMOMO methods.[7]

Density functional theory (DFT), with the hybrid B3LYP[8] exchange and correlation potentials, as defined in the Gaussian94 program,[9] was used for all the calculations reported here. Equilibrium and transition state (TS) structures were determined by gradient optimization. The model systems studied here were too large for force constant calculations. Therefore, at the optimized TS structures, the final iterated Hessian matrix was diagonalized to obtain imaginary eigenvalues. Then, to elucidate the nature of the TS, its geometry was changed in both the forward and the reverse directions of the eigenvector of the imaginary eigenvalue and then released for equilibrium geometry optimizations. This (quasi-IRC) procedure approximates the more rigorous intrinsic reaction coordinate (IRC) method and identifies the reactant and product associated with each TS.

The basis set used is the SBK CEP-31 split-valence set for nitrogen and phosphorus, in conjunction with a compact effective potential (CEP).[10] Analogously, for Zr the small core relativistic CEP (RCEP) and split-valence basis set were used.[10] For the hydrogen atom the standard 31G basis set was used. As was done previously,[6] based on theoretical considerations and actual testing, a set of d-functions with exponent 0.8 was added to the bridging nitrogen atoms.

3. Results and Discussion

All the calculated structures and their relative energies on the potential energy surface of the initial **A7** + H_2 and **B11 (A3)** + H_2 reactions are shown in Figures 2 and 3 (where **A7** will be called **B1**) and in Figures 4 and 5 (where **A3** will be called **B11**), respectively. The structures and relative energies for the complexes involved in the addition of the third H_2 molecule are displayed in Figure 6. Below we will mainly discuss the geometries and energetics calculated with the Zr−P bonds constrained at 2.80 Å. In general, the main conclusions are the same for the Zr−P constrained and unconstrained calculations, and therefore, unconstrained results will be discussed only for a few specific cases.

(7) Yates, B. F.; Basch, H.; Musaev, D. G.; Morokuma, K. To be published.

(8) (a) Becke, A. D. *J. Chem. Phys.* **1993**, *98*, 5648. (b) Lee, C.; Yang, W.; Parr, R. G. *Phys. Rev.* **1988**, *B37*, 785. (c) Stephens, P. J.; Devlin, F. J.; Chabalowski, C. F.; M. J. Frisch, M. J. *J. Phys. Chem.* **1994**, *98*, 11623.

(9) Frisch, M. J.; Trucks, G. W.; Schlegel, H. B.; Gill, P. M. W.; Johnson, B. G.; Robb, M. A.; Cheeseman, J. R.; Keith, T. A.; Petersson, J. A.; Montgomery, J. A.; Raghavachari, K.; Al-Laham, M. A.; Zakrzewski, V. G.; Ortiz, J. V.; Foresman, J. B.; Cioslowski, J.; Stefanov, B. B.; Nanayakkara, A.; Challacombe, M.; Peng, C. Y.; Ayala, P. Y.; Chen, W.; Wong, M. W.; Andres, J. L.; Replogle, E. S.; Gomperts, R.; Martin, R. L.; Fox, D. J.; Binkley, J. S.; DeFrees, D. J.; Baker, J.; Stewart, J. J. P.; Head-Gordon, M.; Gonzales, C.; Pople, J. A. *Gaussian 94*; Gaussian Inc.: Pittsburgh, PA, 1995.

(10) (a) Stevens, W. J.; Basch, H.; Krauss, M. *J. Chem. Phys.* **1984**, *81*, 6026. (b) Stevens, W. J.; Krauss, M.; Basch, H.; Jasien, P. G. *Can. J. Chem.* **1992**, *70*, 612.

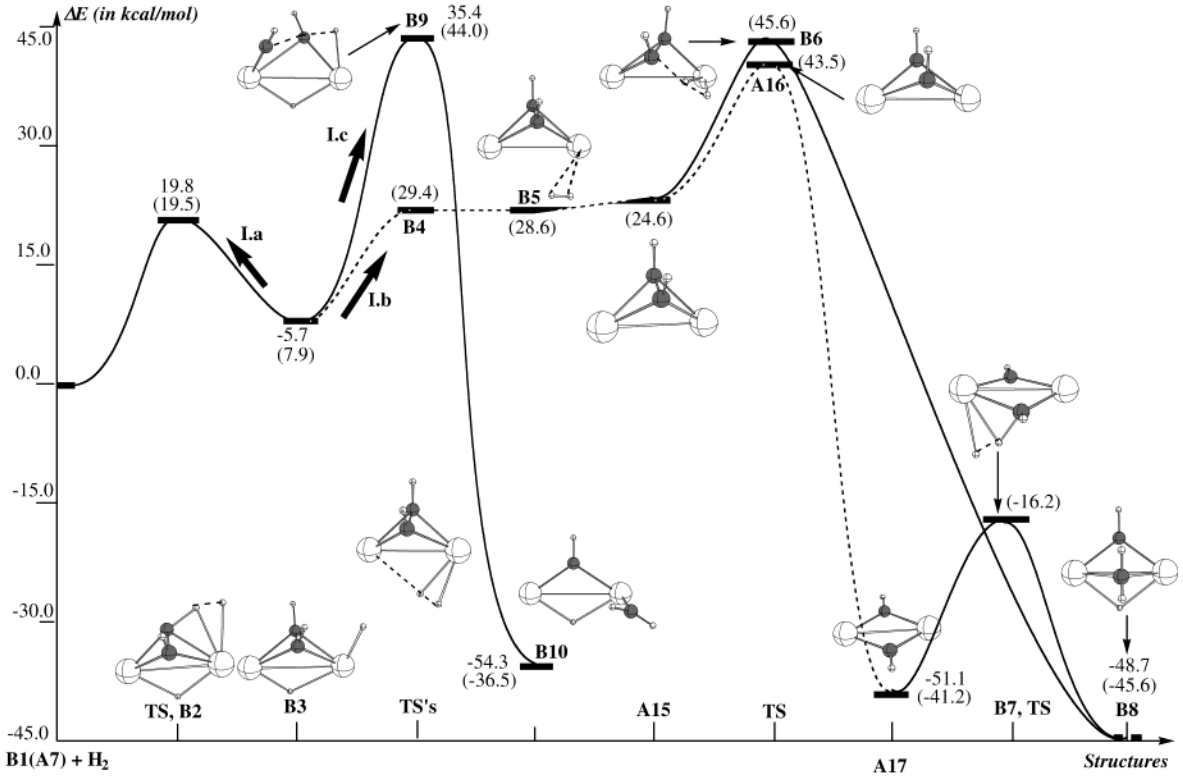

Figure 3. Calculated potential energy profile of the reaction **B1** (**A7**) + H_2, the addition of the second hydrogen molecule to the Zr(μ-N_2)Zr core of the complex **A1**. Numbers given in parentheses were obtained upon constraining the Zr−P bond distances at 2.80 Å.

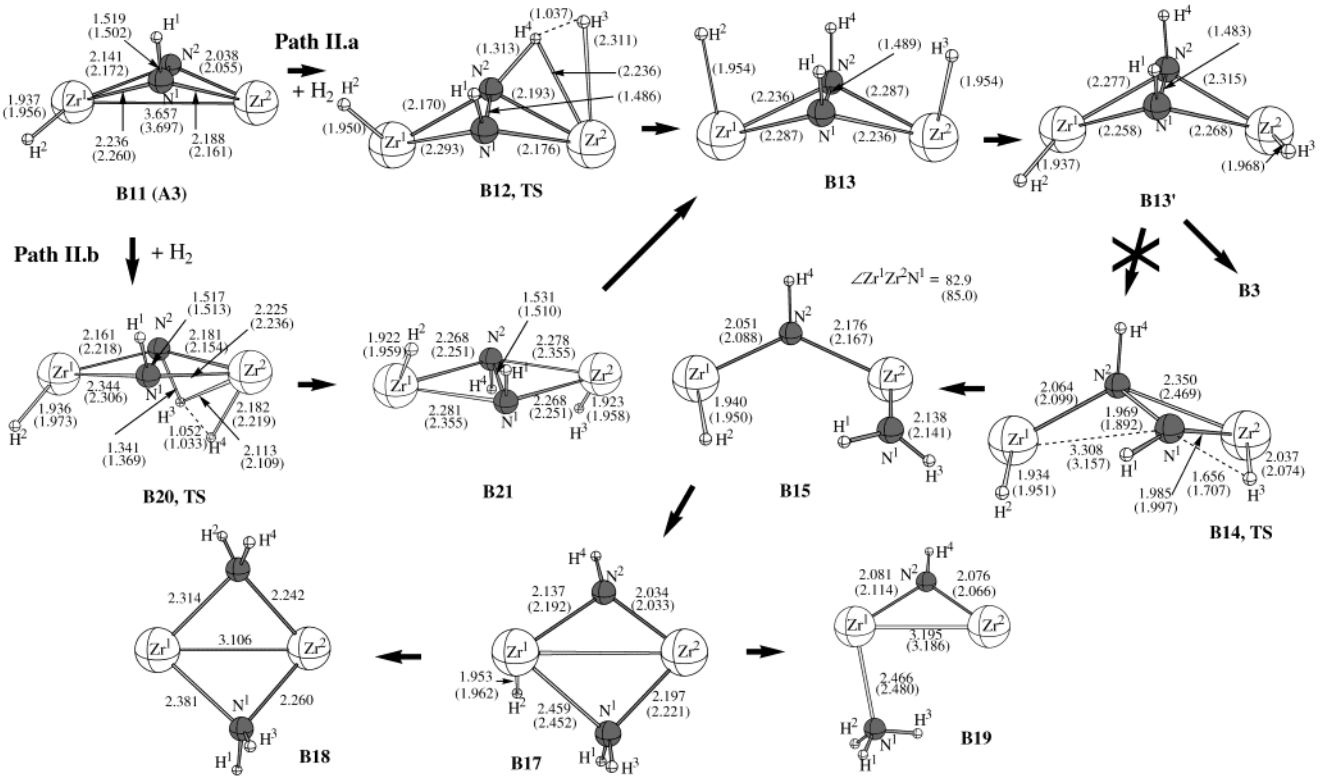

Figure 4. Calculated geometries (distances in Å, angles in deg) of the reactants, intermediates, transition states, and products of the reaction **B11** (**A3**) + H_2, the addition of the second hydrogen molecule to the Zr(μ-N_2)Zr core of the complex **A3**. For clarity, the ancillary PH_3 and NH_2 ligands are omitted. Numbers given in parentheses were obtained upon constraining the Zr−P bond distances at 2.80 Å.

A. Reaction of Complex B1 with the Second H_2 Molecule. Addition of H_2 to B1. The first step of the reaction of H_2 with **B1 (A7)**, [p_2n_2]Zr(μ-η^2-NNH)(μ-H)-Zr[p_2n_2], is coordination of a hydrogen molecule, which takes place only when H_2 approaches from above to the atoms N^2, Zr^1, and Zr^2, shown in Figure 2. This

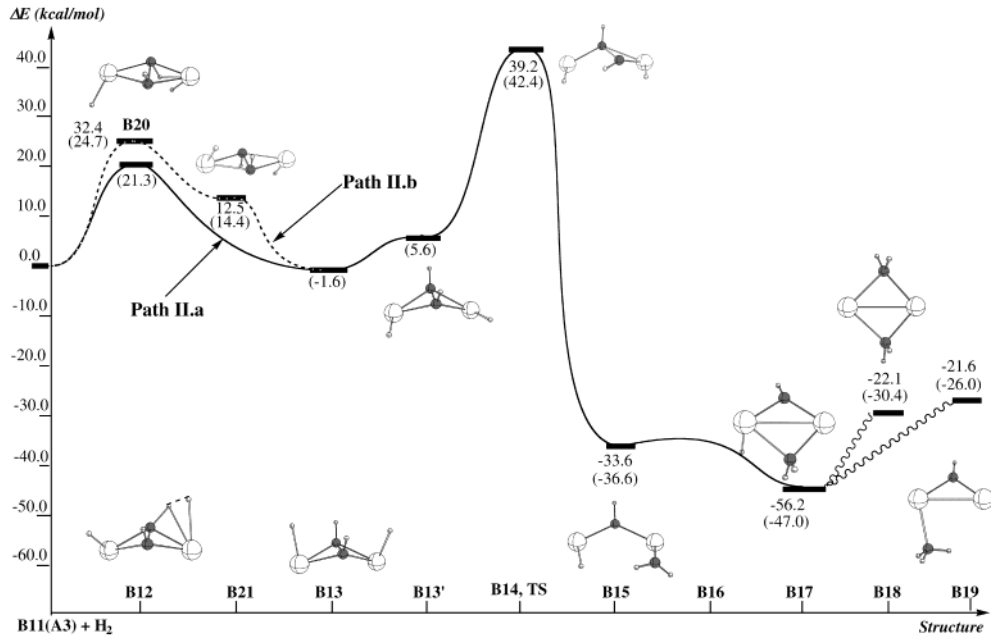

Figure 5. Calculated potential energy profile of the reaction **B11** (**A3**) + H_2, the addition of the second hydrogen molecule to the $Zr(\mu\text{-}N_2)Zr$ core of the complex **A3**. Numbers given in parentheses were obtained upon constraining the Zr−P bond distances at 2.80 Å.

approach leads to the formation of a weakly bound molecular complex (not shown in Figure 2), (H_2)**B1**, which is only 1.2 kcal/mol more stable than reactants, H_2 + **B1**. This loose complex has a Zr^2-H^4 separation of ∼3.4 Å and a N^2-H^4 distance of ∼2.6 Å. Such a loosely bound complex would not exist when entropy is considered. Its existence/nonexistence has no effect on the sequence of reaction steps described below.

The next step of the reaction is the addition of the H^3-H^4 bond to the Zr^2-N^2 bond via transition state **B2**, shown in Figure 2. The geometric character of this TS is very similar to that of **A2**, the TS for addition of the first H_2 molecule.[6] The active site $Zr^2\cdots H^3\cdots H^4\cdots N^2$ bond distances are 2.217 (2.219) Å ($Zr^2\cdots H^3$), 1.020 (1.018) Å ($H^3\cdots H^4$), 1.315 (1.317) Å ($H^4\cdots N^2$), and 2.318 (2.320) Å (Zr^2-N^2) (where the values in parentheses are calculated with the Zr−P constraint), vs 2.266 Å, 1.044 Å, 1.298 Å, and 2.180 Å, respectively, for **A2**. The differences between the Zr−P constrained and unconstrained optimized structures in these bond distances in **B2** are not larger than 0.003 Å. The similarity between the geometries of the TS for the first (**A2**) and second (**B2**) H_2 additions is reflected also in the calculated barrier heights, which are ∼21.2 and 19.8(19.5) kcal/mol for the reactions **A** (in Figure 1) and **B** (in Figure 3), respectively, relative to the corresponding reactants **A1** + H_2 and **B1** + H_2.

Quasi-IRC calculations show that TS **B2** connects molecular complex (H_2)**B1** with oxidative addition product **B3**, $[p_2n_2]Zr(\mu\text{-}\eta^2\text{-}cis\text{-}HNNH)(\mu\text{-}H)Zr(H)[p_2n_2]$. Structure **B3** is calculated to be 5.7 kcal/mol lower in the Zr−P unconstrained but 7.9 kcal/mol higher in the Zr−P constrained geometry optimization, respectively, than the corresponding reactants. This difference in the energy of **B3** for different optimization schemes reflects added crowding about the Zr^2 atom in **B3**. With the new Zr^2-H^3 bond, Zr^2 becomes roughly seven-coordinated. Thus, the $Zr^2-N^1(H^1)$ bond goes from 2.181 Å (**B1**) to 2.209 Å (**B2**) to 2.272 Å (**B3**). The Zr^2-N^2 bond, across which H^3-H^4 is adding, changes to an even larger extent, 2.122 Å (**B1**) → 2.320 Å (**B2**) → 2.317 Å (**B3**). Again, as noted before in reaction **A1** + H_2,[6] the bridging N−N bond distance changes by only ∼0.02 Å. This small decrease probably reflects a slight strengthening of the bridging N−N bond due to weakening of the Zr−N bonds, even though a new N^2-H^4 bond is formed eclipsed with the existing N^1-H^1 bond in **B3**. The results obtained by the unconstrained calculations are very close to those presented above for the constrained calculations. Exceptions are the Zr^1-H^2 and Zr^2-H^2 bond distances. In the constrained calculations, the Zr^2-H^2 bond distance expands from 2.212 Å in **B1** to 2.305 Å in **B3**, while the Zr^1-H^2 bond distance decreases from 2.047 Å in **B1** to 2.011 Å in **B3**. Thus, in **B3** the Zr "bridging" hydrogen atom becomes an almost localized Zr^1-H^2 bond, balancing the new Zr^2-H^4 bond. In contrast, in the unconstrained calculations, Zr^2-H^2 bond distance decreases from 2.223 Å (**B1**) to 2.138 Å (**B3**), and the Zr^1-H^2 bond distance does not change at all. The calculated differences between the unconstrained and constrained calculations are the results of the dissociation of one of the unconstrained phosphine ligands at the Zr^2 center to make room for the new Zr^2-H^3 bond.

The approach conformation in **B2** naturally produces intermediate **B3**, with the new Zr−H and N−H bonds aligned parallel on the outwardly bent face of the Zr_2N_2 core, as in the case of **A3** and the first H_2 addition. However, the energetics of the reactions **A1**+ H_2 → **A3** and **B1** + H_2 → **B3** are slightly different; with the constrained optimization, the former is exothermic by 4.9 kcal/mol, while the latter is endothermic by 7.9 kcal/mol, which, as explained above, is due to the "crowding" around (approximately seven-coordinate) Zr^2 in **B3**.

Reactions of B3. From intermediate **B3**, the reaction in general may proceed via three different pathways: **I.a**, **I.b**, and **I.c**, which will be discussed separately.

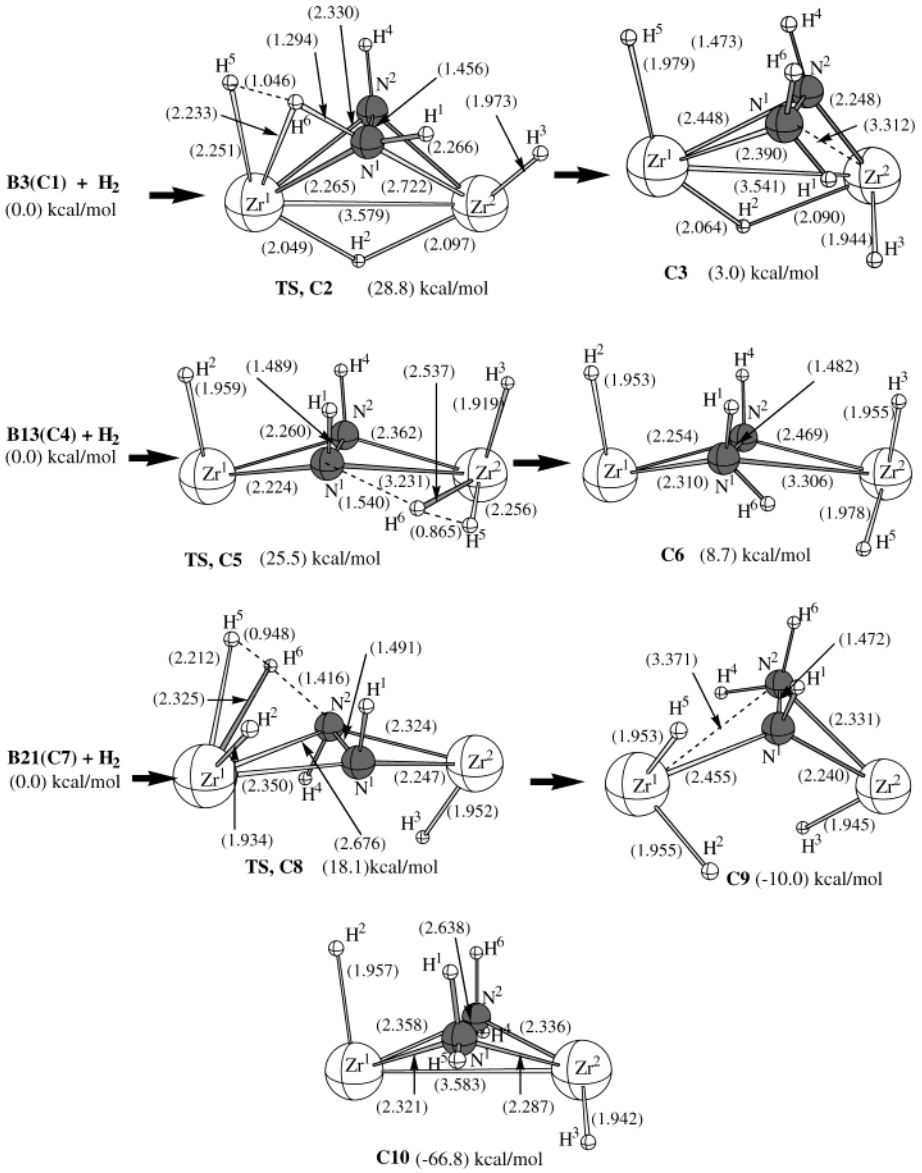

Figure 6. Calculated geometries (distances in Å, angles in deg) and energetics (in kcal/mol) of the transition state and product of the reaction **B3 (C1)** + H_2, **B13 (C4)** + H_2 and **B21 (C7)** + H_2, the addition of the third hydrogen molecule to the Zr(μ-N_2)Zr core of the complex **A1**, at the fixed Zr−P = 2.80 Å bond distances. For clarity, the ancillary PH_3 and NH_2 ligands are omitted.

Path I.a. Path **I.a** is a reverse reaction leading to reactants **B1** + H_2. It takes place with a 11.6 kcal/mol barrier and is exothermic by 7.9 kcal/mol.

Path I.b. The second pathway, path **I.b**, is also a dihydrogen elimination process which involves, as seen in Figure 2, migration of the bridging H^2 ligand to Zr^2 (and H^3) through transition state **B4** to form **B5**, [p_2n_2]-Zr(μ-η^2-*cis*-HNNH)Zr(η^2-H_2)[p_2n_2]. At transition state **B4**, H^2 has already moved to the Zr^2 center from the bridging position between Zr atoms in **B3** and has almost formed the H^2−H^3 bond at 0.880 Å. Quasi-IRC calculations from **B4** confirm that this transition state connects **B3** and **B5**. This reaction occurs with a 21.5 kcal/mol barrier and is about 21 kcal/mol endothermic relative to complex **B3** (see Figure 3). **B5** is a weak H_2 molecular complex with the Zr(μ-η^2-HNNH)Zr core and has a noncoplanar Zr−Zr−N−N structure, as in **B1**, with the N−N bond preserved. The H_2 molecule can dissociate easily to give complex **A15**, [p_2n_2]Zr(μ-η^2-*cis*-HNNH)Zr[p_2n_2], which has been discussed in detail in our previous paper.[6]

As shown in Figure 3, from **A15** the reaction splits into two paths. The first, which has been partially discussed in our previous paper[6] (see also Figure 1), starts with cleavage of the N−N bond via transition state **A16** and leads to the formation of [p_2n_2]Zr(μ-HN)$_2$-Zr[p_2n_2], **A17**, with a coplanar Zr(μ-NH)$_2$Zr core. The process **A15** → **A17** occurs with about 20 kcal/mol barrier (for unconstrained optimization) and is exothermic by 65.8 kcal/mol. However, complex **A17** is not the energetically most favorable product of the reaction **B1** (**A7**) + H_2 of the reaction started from complex **B3**. Indeed, complex **A17** may coordinate and activate a second hydrogen molecule (if it is still available) at transition state **B7** and lead to formation of the thermodynamically most favorable product, [p_2n_2]Zr(μ-NH)-(μ-NH_2)(μ-H)Zr[p_2n_2], **B8**. Our quasi-IRC calculations confirmed **B7** as TS for H−H addition, which also can

be seen by analyzing its geometrical parameters. Indeed, at TS **B7** the H−H bond is elongated to 0.997 Å, and the formed Zr^1-H^2 and N^1-H^3 bonds shrink to 2.200 and 1.375 Å, respectively. However, according to the quasi-IRC calculations, transition state **B7** does not connect directly to reactants **A17** + H_2 with complex **B8**; instead, it connects to the weakly bound **A17**(H_2) molecular complex (not presented in Figures 2 and 3) with the complex **B8′** (not presented in Figures 2 and 3) having a (H)Zr(μ-NH)(μ-NH_2)Zr core. The **B8′** → **B8** isomerization, corresponding to migration of a H atom (atom H^2) from a terminal (coordinated to only one of Zr centers) to a bridging (coordinated to both Zr centers) position, is expected to be a kinetically easy process and has been discussed in our previous paper.[6]

As seen in Figure 3, complex **B8** with the Zr(μ-NH)(μ-NH_2)(μ-H)Zr core is calculated to be 48.7(45.6), 43.0(53.5), and (65.6) kcal/mol lower in energy than reactants **B1** (**A7**) + H_2, **B3**, and **A15** + H_2, respectively. Process **A17** + H_2 → **B8** is found to be 2.3 kcal/mol endothermic, but 4.4 kcal/mol exothermic in the unconstrained and constrained Zr−P calculations, respectively. Both $Zr-N^1(H)$ distances are 2.119 Å, while the $Zr-N^2(H_2)$ distances are 0.23 Å larger (see Figure 2), as expected from the weaker bonds to a tetrahedral N^2 atom. The bridging Zr^1-H^2 and Zr^2-H^2 bonds are both 2.082 Å. As noted above, the Zr−Zr distance is short, 3.179 Å, and the N−N bond is completely broken at an internuclear distance of 2.778 Å. The three bridging ligands (N^1H, N^2H_2, and H^2) bring the two Zr atoms closer, and the absence of a N−N bond concentrates the bonding between the bridging N atoms and the Zr atoms.

Thus, the process from **B3** with the Zr(μ-η^2-*cis*-HNNH)(μ-H)Zr core + H_2 → TS **B4** → **B5** → (−H_2) → **A15** → TS **A16** → **A17** → (+H_2) → TS **B7** → **B8** occurs with about 21.5, 18.9, and 25.0 kcal/mol barriers at TS's **B4**, **A16**, and **B7**, respectively.

The most important finding in this subsection is that a pathway has been found to convert **B1 (A7)**, $[p_2n_2]Zr(\mu\text{-}\eta^2\text{-}NNH)(\mu\text{-}H)Zr[p_2n_2]$, to complex **A17** with the Zr(μ-$NH)_2$Zr core, by the aid of the second reacting hydrogen molecule. In our previous paper,[6] we studied reaction of $[p_2n_2]Zr(\mu\text{-}\eta^2\text{-}N_2)Zr[p_2n_2]$, **A1,** with the first H_2 and showed that, while the complex $[p_2n_2]Zr(\mu\text{-}NH)_2Zr[p_2n_2]$, **A17**, is thermodynamically the most stable product of the reaction, and even more stable than the experimentally observed product **A7** (**B1**), it cannot be generated during the reaction of **A1** + H_2 because of the existence of a very high barrier (about 55 kcal/mol) for unimolecular rearrangement of **A7** to **A17**. However, our new results presented above point to both the kinetic and thermodynamic feasibilities of the formation of complex **A17**. Addition of H_2 to $[p_2n_2]Zr(\mu\text{-}\eta^2\text{-}NNH)Zr[p_2n_2](\mu\text{-}H)$, **B1**(**A7**), followed by re-elimination of H_2, gives **A15**, which can be converted into the thermodynamically most favorable product **A17**, with overall barriers of about 20 kcal/mol at TS **B2** (for the second H_2 addition) and at TS **A16**.

A second process that can start from **A15** is the coordination and activation of a second H_2 molecule, which leads to complex Zr(μ-NH)(μ-NH_2)(μ-H)Zr, **B8**. This process is exothermic by about 21 kcal/mol and occurs with a 21.0 kcal/mol barrier at TS **B6**. As seen in Figure 2, at the transition state **B6** the broken H^2-H^3 bond is elongated to 0.917 Å, while the formed Zr^2-H^2 and N^1-H^3 bonds are 2.312 and 3.122 Å, respectively. In other words, the H−H activation takes place mainly on one of the Zr centers, followed by migration of H^3 to N^1. This localization is caused by the existence of the N−N bond in TS **B6**, compared with its absence in TS **B7**. Once again, quasi-IRC calculation shows that TS **B6** connects reactants **A15** + H_2 (more precisely, a weakly bound **A15**(H_2) complex not presented in Figures 2 and 3) with complex **B8′** (also, not presented in Figures 2 and 3), having the (H)Zr(μ-η^2-NH)(μ-η^2-NH_2)-Zr core. As discussed above, **B8′** can rearrange into complex **B8** with a small energetic barrier (not studied in this paper) via migration of the H^2 atom from a terminal to a bridging position.

Although both processes (the N−N bond cleavage leading to **A17** followed by H_2 addition to give **B8** and the direct H_2 addition leading to **B8**) starting from **A15** occur with moderate energetic barriers and are exothermic, the process via **A17** looks slightly more favorable. Since the calculated rate-determining barriers for both processes starting from **A15** are comparable to that corresponding to addition of the first H_2 molecule to **A1**, which is known to occur under laboratory conditions, one expects that the former processes also will be experimentally feasible under appropriate laboratory conditions.

Path I.c. The third pathway, path **I.c** starting from **B3**, involves migration of H^3 from Zr^2 to either of the N^1 or N^2 centers to form the second N−H bond and leads to complex **B10**. The first step of this process, migration of the H^3 atom from Zr^2 to N^2 (or N^1), occurs through TS **B9**. As seen in Figure 2, there is no significant change in the Zr^2-H^3 bond length of 1.982 Å in **B9** compared to its value of 1.977 Å in **B3**. The H^3-N^2 distance in **B9** is 1.577 Å. In this process, the bridging $Zr-H^2-Zr$ bond lengths become more equal (2.116 and 2.026 Å, respectively) as Zr^2 begins to lose its localized Zr^2-H^3 bond in the migration process. The migration of H^3 from Zr^2 to N^2 has two other major consequences. First, the Zr^2-N^1 bond is essentially broken, being elongated to 3.44 Å, with a consequential shortening of the Zr^1-N^1 bond from 2.260 Å in **B3** to 1.965 Å in **B9**. This latter distance can be considered to be double bond length. The second structural feature is the breaking of the N−N bond, where its distance is 1.958 Å in **B9** compared to the normal 1.483 Å in **B3**. The breaking of the N−N bond is an interesting consequence of the increased coordination around N^2. The Zr^1-N^2 bond is also elongated to 2.630 Å in **B9** from 2.163 Å in **B3**, as expected from the incipiently tetracoordinate N^2 in **B9**. The Zr^2-N^2 distance actually contracts from 2.317 Å in **B3** to 2.113 Å in **B9** due to the bridging H^3 atom. The breaking of the Zr^2-N^1 bond in **B9** is temporary, as we will see, and apparently serves to allow the strengthening (shortening) of the Zr^2-N^2 bond needed by the migration process. The calculated barrier for H^3 migration from Zr^2 to N^1 is a substantial 41.1(36.1) kcal/mol relative to the **B3** complex.

The quasi-IRC calculations confirm that TS **B9** connects structures **B3** and **B10**. In complex **B10**, the transfer of H^3 from Zr^2 to N^2 is complete, the Zr^1-N^2 bond is completely broken, and $N^1(H^1)$ reattaches itself

to Zr^2. This re-formation of the latter bond shows that its breakage in **B9** was a temporary expedient to facilitate the main processes. The detachment of the N^1H_2 group from Zr^2 avoids the formation of a four-coordinate N^2 atom. The stability of **B10** is considerable, −54.3(−36.5) kcal/mol relative to reactants (**B1** + H_2).

At the next step, **B10** can be converted to **B8** essentially by the reattachment of N^2 to Zr^1. Additional changes involve the partial rotation of the bridging N^2H_2 group to form a tetrahedral N^2 atom with the two Zr and two H atoms and the contraction of the Zr−Zr bond to 3.179 Å in **B8** from 3.437 Å in **B10**. Complex **B8** is actually nearly exactly symmetric with an approximate reflection plane perpendicular to the Zr−Zr axis on the line of the bridging $N^2-N^1-H^2$ atoms. All our attempts to locate the transition state connecting **B10** and **B8** failed, suggesting that the energetic barrier separating these two structures is small. This conclusion also has been confirmed by partial geometry optimization of the expected transition state between structures **B10** and **B8**. Indeed, starting with structure **B10**, stepping the $N^2-Zr^1-N^2$ distance from 4.281 Å downward in fixed intervals of 0.25 Å, and reoptimization of all other geometry parameters at each fixed Zr^1-N^2 distance give an energy maximum of ∼3 kcal/mol (relative to **B10**) at a Zr^1-N^2 distance of 3.25 Å. Equilibrium geometry optimization starting from such a "TS" structure results in complex **B10**. Stepping the Zr^1-N^2 distance down to 2.50 Å and releasing the Zr^1-N^2 constraint in an equilibrium geometry optimization give **B8**. The conclusion to be drawn from these results is that there probably is a small barrier between **B10** and **B8**, but we were not able to find the TS structure.

The above-presented findings and comparing with our previous results for the **A1** + H_2 reaction[6] indicate that addition of the second hydrogen molecule to **B1** (**A7**) should be as easy as addition of the first H_2 molecule to **A1**, which is known to occur at laboratory conditions. Indeed, the rate-determining barriers of the reaction sequence **A1** + H_2 → **A3** → **A7** and **B1 (A7)** → **B3** are calculated to be 21.2 and 19.8 (19.5) kcal/mol, respectively. However, the first process is exothermic by 13 kcal/mol, while the second process is endothermic by 8 kcal/mol.

From the resultant complex **B3**, the process can proceed via three different paths, **I.a**, **I.b**, and **I.c**. Path **I.a**, corresponding to reverse reaction **B1 (A7)** ← **B3**, is likely to be more preferable because of the lower (11.6 kcal/mol) barrier. Path **I.c** is not feasible because of high, 41.1(36.1) kcal/mol barrier. However, path **I.b** can be competitive with **I.a**; it occurs with a barrier, 21.5 kcal/mol, and leads to **A15**. From **A15** two new processes, the N−N bond cleavage leading to **A17** followed by H_2 addition to give **B8** and the direct H_2 addition leading to **B8**, could start. Although both processes occur with moderate barriers and are exothermic, the process proceeding via the N−N bond cleavage leading to **A17** and then **B8** looks slightly more favorable. Either of these processes should be experimentally feasible under appropriate laboratory conditions. In other words, the direct reaction of $[p_2n_2]Zr(\mu\text{-}\eta^2\text{-}N_2)Zr[p_2n_2]$, **A1**, with the first H_2 molecule cannot produce the thermodynamically most stable product $[p_2n_2]Zr(\mu\text{-}NH)_2Zr[p_2n_2]$, **A17**, because of a very high barrier (about 55 kcal/mol) for unimolecular rearrangement of **A7** to **A17**. However, product **A17**, can eventually be formed by the reaction of the second hydrogen molecule with **A7**.

B. Reaction of Complex B11 with the Second H_2 Molecule. Another reasonable starting point for addition of the second H_2 molecule is $[p_2n_2](H)Zr(\mu\text{-}\eta^2\text{-}NNH)Zr[p_2n_2]$, **A3**, called **B11** below, although this complex has not been observed experimentally. **A3** is expected to quickly convert to **A7,** which has been isolated and characterized. Here, the reaction may proceed via two different paths, **II.a** and **II.b**, which differ by the direction of approach of the attacking dihydrogen. The first of them, **II.a**, corresponds to coordination of the H_2 molecule from above (where there is no Zr−Zr bond, and the N−N bond is protruded and consequently is easily accessible), while the second pathway, **II.b**, involves coordination of H_2 from below, where there is Zr−Zr bond and the N−N bond is sheltered inside. Both of these pathways lead to complexes of the $(H)Zr(\mu\text{-}\eta^2\text{-}HNNH)Zr(H)$ type with two bridging N−H bonds parallel to each other. However, in the first case the N−H bonds are located cis, while in the second case they are trans to each other. Let us discuss these pathways separately.

Path II.a. This path starts by coordination of the H_2 molecule to **B11 (A3)** from the above, where addition of the H−H bond to the Zr^2 and N^2 atoms occurs. In the four-center transition state, **B12**, for this reaction, as seen in the Figure 4, the H^4-H^3 bond to be broken is elongated from 0.743 Å in the free dihydrogen molecule to 1.037 Å, while the forming N^2-H^4 and Zr^2-H^3 bonds are calculated to be 1.313 and 2.311 Å, respectively. Approximate IRC calculations starting from **B12** actually lead to **B11″** + H_2 in the reverse (**B12** → **B11**) direction with the constrained geometry optimization. **B11″** (not presented in Figure 4) is an isomer of **B11**, where the PH_3 ligands are located trans to each other in both Zr^1 and Zr^2. In the forward direction IRC calculations lead to the product complex **B13**, presented in Figure 4. The barrier height from **B11** + H_2 to **B12** is calculated to be 21.3 kcal/mol, which is only ∼2 kcal/mol higher than the **B1** → **B2** path discussed in the previous section. In the product complex **B13** two N−H bonds are located cis to each other. The calculated HN−NH bond distance, 1.489 Å, is very close to that in TS **B12** (1.486 Å) and reactant **B11** (1.502 Å). The Zr^1-H^2 and Zr^2-H^3 distances, both 1.954 Å, are also close to the Zr-terminal hydrogen bond distance, Zr^1-H^2, calculated for the reactant **B11** at 1.956 Å and for TS **B12** at 1.950 Å. The reaction **B11** → **B12** → **B13** is exothermic by 1.6 kcal/mol. Since the calculated barrier at TS **B12** is similar to those for the **A1** → **A2** (see our previous paper[6]) and **B1**→ **B2** processes, and the reaction **B11** → **B12** → **B13** is exothermic, one may expect that **II.a** is a feasible reaction path.

In the next step, H^3 migrates from Zr^2 to N^1. This step can start either from **B13** or from its energetically less stable (by 7.2 kcal/mol) isomer **B13′**, where the PH_3 ligands of the Zr^1 center are positioned cis (while in **B13** they are trans) to each other. Since this step of the reaction is not a crucial one, we studied it only for complex **B13′**. It was found that the migration of H^3 from Zr^2 to N^1 occurs via TS **B14**, where H^3-N^1 is 1.707 Å, Zr^2-H^3 = 2.074 Å, and Zr^1-N^1 and N^2-N^1 are

stretched to 3.157 and 1.892 Å, respectively. Formation of **B14** is accompanied by a breaking of the Zr^1-N^1 and N^1-N^2 bonds, while the Zr^2-N^1 bond shortens to 1.997 Å. The Zr−Zr distance elongates in TS **B14** to 4.155 Å, presumably due to the loss of bridging $Zr-N^1-Zr$ bonding and the use of Zr orbitals for the breaking Zr^2-H^3 bond, which still has a bond length of 2.074 Å in **B14**. The barrier height for the H^3 migration is calculated to be 36.8 kcal/mol, relative to the **B13′.** Again, as in **A8**, **A14**, and **B9**, after the initial H_2 addition and possible bond preserving rearrangements, the subsequent reaction path is effectively blocked by this high barrier.

TS **B14** leads to the complex **B15**. Here all the incipient changes found in TS **B14** are completed: N^1 has two N−H bonds and is essentially localized on Zr^2, and the N−N bond is completely broken. In almost every aspect, **B15** is an analogue to **B10** of the previous reaction path. This is true even energetically; **B15** is 36.6 kcal/mol more stable than reactants (**B1** + H_2) and 79 kcal/mol below TS **B14** in the Zr−P frozen geometries. For the unconstrained structures, the corresponding stabilities are 33.6 and 72.8 kcal/mol. The similarity in developments along the **A** (first H_2) and **B** (second H_2) reaction paths is very clear, both structurally and energetically.

In the final reaction step, the Zr^2-N^1 bond is formed to give **B17**, with N^2-H^4 and N^1-H_2 groups bridging across the two Zr atoms. The localized Zr^1-H^2 bond is preserved but rotated away from Zr^1-N^2 toward the new Zr^1-N^1 bond. The $Zr-N^1$ bond lengths are longer than $Zr-N^2$, because of the higher coordination of N^1. The Zr^1-N distances are longer than Zr^2-N because of the Zr^1-H^2 bond. The N^1-N^2 bond is a completely broken at 2.864 Å, while Zr^1-Zr^2 shortens to 3.364 Å, characteristic of Zr−Zr distances in these complexes when the bridging N atoms are not bonded to each other. The exothermicity of **B17** is 47.0 kcal/mol in the frozen Zr−P distance geometry relative to reactants and 9.4 kcal/mol relative to **B15**. TS **B16**, representing the incipient closing of the Zr^2-N^1 bond and rotation of the Zr^1-H^2 bond, has not been found. The barrier for this process is expected to be small.

We also have calculated the products of migration of the terminal H^2 ligand in **B17** from Zr^1 to N^2H and to $N^1H^1H^3$, which are $Zr(\mu\text{-}NH_2)_2Zr$, **B18**, and $(NH_3)Zr(\mu\text{-}NH)Zr$, **B19**, respectively. Since these processes are endothermic, by 17 and 21 kcal/mol, respectively, we did not explore the intermediate structures and transition states.

The above presented results show that path **II.a**, **B13** → **B13′** → **B14** → **B15** → ..., is kinetically unfavorable and unlikely to proceed further. However, the alternative pathway starting from **B13** or **B13′** and leading to complex **B3**, the direct product of the **B1** (**A7**) + H_2 reaction, is likely to be feasible. Indeed, **B13** and **B13′** are isomers of the complex **B3**. They lie 1.4 kcal/mol lower and 4.2 kcal/mol higher than **B3**, respectively, and are probably connected by a TS for rotation of the Zr^1H^2 group around the Zr^1-N bonds (possibly as seen in **B13′**) or migration of H^2 from the position cis to the NH bonds to the trans position. Although we did not study this process carefully, one may assume that **B13** can be converted to **B3** and continue alone the allowed path mapped for **B3** in Figures 2 and 3.

Path II.b. The second pathway for the reaction **B11 (A3)** + H_2 leads to complex **B21**, where the N−H bonds are trans to each other. It takes the now familiar path: addition of H_2 across the Zr^2-N^2 bond, where the original hydrogen atoms are in the N^1-H^1 and Zr^1-H^2 bonds. TS **B20** for this reaction involves four atoms, Zr^2, N^2, H^3, and H,[4] in the active regions and has the typical bond distances: $N^2-H^4 = 1.369$ Å, $H^3-H^4 = 1.033$ Å, $H^3-Zr^2 = 2.219$ Å, and $Zr^2-N^2 = 2.154$ Å. The last bond length is normal, while typical equilibrium bond distances for the others are N−H = 1.035 Å, H−H = 0.74 Å, and H−Zr = 1.95 Å. The barrier height from **B11 (A3)** + H_2 to **B21** is 32.4(24.7) kcal/mol at the TS **B20**. The ∼7 kcal/mol difference in the barrier height is mainly due to **B11 (A3)**, which is destabilized more than **B20** under the Zr−P constraint. Of course, this "destabilization" represents the constraints of the $[P_2N_2]$ ligand and should give more realistic energetics. Thus, 24.7 kcal/mol is the barrier height, which is ∼5 and 3.5 kcal/mol higher than the **B1** → **B2** and **B11** → **B12** barriers, respectively. The calculated difference is not sufficiently large to rule out this path as experimentally unfeasible.

TS **B20** leads to complex **B21**. Here, the N−H and Zr−H bonds form a relatively symmetric geometry, moderated by the eclipsed nature of pairs of N−H and Zr−H bonds. Thus, Zr^2-N^2 is 2.355 Å and Zr^1-N^2 is 2.251 Å. The same difference is found for the Zr^2-N^1 and Zr^1-N^1 bond lengths. It should be noted that the N^1-N^2 bond length is hardly affected on going from **B11** to **B20** to **B21**; all three distances being within 0.005 Å of each other. This has been found and explained for the previous H−H additions across Zr−N. The two N−H bonds in **B21** are trans to each other across the N^1-N^2 bond. This trans conformation does not allow hinging at the N^1-N^2 axis that would allow a stronger Zr−Zr bonding interaction. Therefore, the Zr_2N_2 core in **B21** is essentially planar and the Zr−Zr distance is long at 4.353 Å. This distance can be compared with the corresponding value in **A3** (3.697 Å) and in **B3** (3.558 Å). The latter is the product of **A7** + H_2 and is strongly hinged at the N^1-N^2 axis, which is allowed by the two N−H bonds having a cis conformation.

Reaction product **B21** is calculated to be 12.5(14.4) kcal/mol above **B11** + H_2. This energy difference is higher than **B3** relative to **B1** + H_2 and **B13** relative to **B11** + H_2 and again indicates that **B11** → **B21** is probably less favorable than **B1** → **B3** and/or **B11** → **B13.** The approximate IRC starting from the TS actually leads to **B11′** (not presented in Figure 4) + H_2 in the reverse (**B20** → **B11**) direction. **B11′** (**A3′** in our previous paper[6]) closely relates to **B11** and differs from that mainly by having the Zr^1-H^2 bond rotated from being approximately parallel to N^1-H^1 to approximately perpendicular to N^1-H^1 and tilted upward toward the $[p_2n_2]$ cluster on Zr^1. **B11′** is 1.9(1.3) kcal/mol less stable than **B11**. The structure **B11′**, more likely, is an artifact of the simple $[p_2n_2]$ model for the macrocyclic ligand (for detail see our previous paper).[6] In any event, given the similarity in structure and energy of **B11** and **B11′**, we treat them as equivalent, from the point of view of the reaction path. In the forward direction (**B20** → **B21**), the unconstrained geometry optimization leads directly to **B21**, but the Zr−P frozen optimization leads to a form

of **B21** (**B21′**, not shown in Figure 4) having one Zr−H bond rotated away from being eclipsed with an N−H bond toward alignment with the N^1-N^2 bond axis. **B21′** is ∼6 kcal/mol more stable than **B21**, due to the alleviation of one eclipsed Zr−H/N−H interaction. However, in **B21′**, the orientation of the $[p_2n_2]$ ligands on the Zr with the rotated Zr−H bond has the two PH_3 groups cis to each other, rather than trans as in the real $[P_2N_2]$ ligand. The **B21** structure, although more stable than **B21′**, would then seem to be an artificial result of the unconnected $[p_2n_2]$ model in place of the macrocyclic $[P_2N_2]$. From the reaction path point of view, we treated structures **B21** and **B21′** as the same. Therefore, one concludes that the approximate IRC in both the forward and reverse directions from TS **B20** leads to **B11** (**B11′**) and **B21** (**B21′**), respectively.

The next stage of the reaction mechanism is the motion connecting **B21** with the two bridging N−H bonds trans to each other to **B13** with cis N−H bonds. **B13** is calculated to be more stable than **B21** by 16.0 kcal/mol in the Zr−P frozen structures. This stabilization can be explained in terms of the stronger Zr···Zr interaction in **B13**, which also resulted in the "bent" eclipsed conformation. Indeed, the Zr···Zr distance is found to be much longer in the staggered conformation than the eclipsed one. The barrier(s) for **B21** → **B13** can be expected to be small. As pointed out above, in **B13** the Zr_2N_2 core is hinged at the N^1-N^2 axis. Because of this difference between **B21** and **B13**, it is difficult to assess the degree of motion of the $[p_2n_2]$ ligands, if any, on going from **B21** to **B13**. The Zr−N and N−N bond distances do not change much from **B21** to **B13**, as expected from the preservation of all the bond types. The Zr−Zr distance decreases from 4.353 to 3.970 Å (**B13**) due to the hinged bending of the Zr_2N_2 core.

Thus, the above presented results show that the addition of the second hydrogen molecule to **B11** takes place via path **II.a**, which is kinetically and thermodynamically more favorable than path **II.b**. Indeed, reaction **B11** + H_2 → **B13**, path **II.a**, occurs only with the 21.3 kcal/mol barrier and is endothermic by 5.6 kcal/mol. In contrast, reaction **B11** + H_2 → **B21**, path **II.b**, requires 24.7 kcal/mol and is endothermic by 14.4 kcal/mol. However, in both cases the reverse reactions, **B13** → **B11** + H_2 and **B21** → **B11** + H_2, respectively, which occur with only 15.7 and 10.3 kcal/mol barriers and are exothermic (by 5.9 and 14.4 kcal/mol, respectively), will occur more easily, and the addition of the H_2 molecule to complex **B11**(**A3**) has to compete against this process.

C. Addition of the Third H_2 Molecule to Complexes B3, B13, and B21. The complexes that can be starting points for addition of the third molecule of H_2 are **B3** (which we call **C1**), **B13** (**C4**), and **B21** (**C7**). Because of atomic congestion, only Zr−P frozen structures were optimized for the expected TS's and products of these reactions.

Reaction of B3 (C1) with a H_2 Molecule. Let us start our discussion from the reaction of **C1** with a dihydrogen molecule. As seen in Figure 6, the addition of H_2 to **C1** occurs across a Zr−N bond. Reactant **C1** has Zr^2-H^3, N^1-H^1, N^2-H^4, and $Zr^1-H^2-Zr^2$ bonds. The third H_2 molecule can then attach to the hydrogen-bare Zr^2 and one of the bridging nitrogen atoms (N^1 in our case) to form a $N^1\cdots H^6\cdots H^5\cdots Zr^1$ ring. As seen for TS **C2**, active site internuclear distances have their usual values: $H^5-H^6 = 1.048$ Å, $H^6-N^1 = 1.294$ Å, and $H^5-Zr^1 = 2.251$ Å. The last value is somewhat longer than in such TS's discussed in earlier sections, probably because of the additional general crowding of a larger number of atoms. The Zr^2-N^1 bond is elongated to 2.722 Å because of the high coordination around N^1. The Zr^1-N^1 distance is constrained by the active site ring. The Zr−Zr distance is 3.579 Å, typical for systems with a bridging Zr−H−Zr bond. The N^1-N^2 bond is preserved at 1.456 Å. The product of reaction **C1** + H_2 is **C3**. Each Zr atom has a Zr−H bond, but Zr^1-H^5 is longer because of stronger bonding of Zr^1 to N^1. The Zr^2-N^1 bond is broken at 3.312 Å, but the N^1-N^2 bond is maintained at 1.473 Å. The Zr−Zr distance is essentially unchanged in the **C1** → **C2** → **C3** transformation. The barrier height at **C2** is calculated to be relatively high, 28.8 kcal/mol. **C3** is calculated to be 3 kcal/mol above the reactants (**C1** + H_2).

Reaction of B13 (C4) with a H_2 Molecule. Starting from **C4**, addition of the third dihydrogen molecule takes place, as expected, across one of the two longer Zr−N bonds. As seen in Figure 6, in TS **C5**, the dihydrogen H^5-H^6 bond being broken is elongated to 0.865 Å. Meantime the forming H^6-N^1 and Zr^2-H^5 bonds are found to be 1.540 and 2.256 Å, respectively. These values of the forming and breaking bonds during the reaction clearly indicate an early (reactant-like) character of TS **C5**. At **C5**, the Zr^1-N^1 and Zr^2-N^2 bond distances have changed only slightly, while, as expected, the Zr^2-N^1 and Zr^2-N^2 bond distances changed significantly; the first of them is completely broken, while the other is elongated by 0.13 Å. The N^1-N^2 bond is preserved at 1.489 Å. The product **C6** has a completely broken Zr^1-N^1 bond, but the N^1-N^2 bond is preserved at 1.482 Å. Zr^2 has two Zr−H bonds and Zr^1 has only one. The **C4** → **C6** reaction is calculated to be 8.7 kcal/mol endothermic. The barrier height at **C5** is calculated to be 25.5 kcal/mol.

Reaction of B21 (C7) with a H_2 Molecule. As shown above, **C7** has the same type and number of bonds as **C4** and differs only in conformation and is 16 kcal/mol less stable than **C4 (B13)** (see Figures 4 and 5). One may expect that the products of reaction **C7** and **C4** with another H_2 molecule also will be different from each other by conformational changes. Therefore, we will not discuss the geometries of transition state **C8** and product **C9**. Here, we would only like to point out that the **C7** + H_2 → **C8** → **C9** reaction takes place with an 18.1 kcal/mol barrier and is exothermic by 10.0 kcal/mol.

We did not investigate possible processes starting from **C3**, **C6**, and **C9**. However, we have calculated complex **C10** with the $(H)Zr(\mu\text{-}NH_2)_2Zr(H)$ core, which can be a result of multiple (or single) rearrangements of complexes **C3**, **C6**, and **C9**. As seen in Figure 6, the main structural features of **C10** are two bridging NH_2 groups and a terminal hydrogen atom on each Zr center. The calculated N−N distance, 2.638 Å, in **C10** is significantly longer than that for structures **C3**, **C6**, and **C9**, and thus the N−N bond is completely broken in **C10**. **C10** is calculated to be significantly lower in energy than **C3**, **C6**, and **C9**; for example, it lies about 55.1 kcal/mol lower than **C9.**

In summary, we note that, for **B3 (C1)** and **B13 (C4)**, the thermodynamically most favorable products of the addition of two H_2 molecule to **A1**, the calculated barrier heights of reactions with the third H_2 molecule are a few kcal/mol larger than those for the first and the second H_2 addition processes we reported earlier[6] and above. Therefore, by adjusting the reaction conditions or by optimizing ligands, the reaction of the third H_2 molecule may be possible.

4. Conclusions

We have presented the results of density functional studies of the reaction mechanism of the model complexes $[p_2n_2]Zr(\mu\text{-}\eta^2\text{-}N_2)Zr[p_2n_2]$, **A1**,[6] $[p_2n_2]Zr(\mu\text{-}\eta^2\text{-}NNH)(\mu\text{-}H)Zr[p_2n_2]$, **B1 (A7)**, $[p_2n_2](H)Zr(\mu\text{-}\eta^2\text{-}NNH)Zr[p_2n_2]$, **B11 (A3)**, $[p_2n_2]Zr(\mu\text{-}\eta^2\text{-}cis\text{-}HNNH)(\mu\text{-}H)Zr(H)[p_2n_2]$, **C1 (B3)**, $[p_2n_2](H)Zr(\mu\text{-}\eta^2\text{-}cis\text{-}HNNH)Zr(H)[p_2n_2]$, **C4 (B13)**, and $[p_2n_2](H)Zr(\mu\text{-}\eta^2\text{-}trans\text{-}HNNH)Zr(H)[p_2n_2]$, **C7 (B21)**, with a molecule of hydrogen. From these studies, one may draw the following conclusions.

1. Reaction of model complex, **A1**, $[p_2n_2]Zr(\mu\text{-}\eta^2\text{-}N_2)Zr[p_2n_2]$, where $[p_2n_2] = (PH_3)_2(NH_2)_2$, with a hydrogen molecule proceeds via a 21 kcal/mol barrier at the "metathesis-like" transition state, **A2**, for the H−H bond activation and produces the diazenidohydride complex, **A3**, and the diazenido-μ-hydride complex, **A7**.[6] Complex **A7** lies a few kcal/mol lower than **A3** and is the only observed product of the experimental analogue of the calculated **A1** + H_2 reaction. However, the experimentally observed diazenido-μ-hydride complex, **A7**, is not the lowest energy structure on the reaction path. The hydrazono complex **A13** with a bridging NH_2 and the hydrado complex **A17** with two bridging NH units are calculated to be more stable than **A7** by about 40−50 kcal/mol. However, these complexes cannot be generated by the reaction of **A1** + H_2 at ambient conditions because of very high (nearly 55−60 kcal/mol) barriers at **A10** and **A14** separating them from **A7**.

2. The addition of a hydrogen molecule to **B1** (**A7**), the experimentally observed product of the reaction **A1** + H_2, can take place to give product **B3** with a 19.5 kcal/mol barrier, which is 1.2 kcal/mol smaller than that for the **A1** + H_2 → **A7** reaction. Since the addition of the first H_2 molecule to **A1** is known to occur at laboratory conditions, one predicts that the addition of the second hydrogen molecule to **A1** (or the addition of the H_2 molecule to **B1** (**A7**)) should also be feasible.

3. From the product **B3**, which lies 7.9 kcal/mol higher than reactants **B1** + H_2, the process will most likely proceed via either channel **I.a** (the reverse dihydrogen elimination reaction **B3** → **B1** + H_2) or channel **I.b** (another dihydrogen elimination process, **B3** → **A15** + H_2); both processes have relatively moderate barriers, 11.7 and 21.5 kcal/mol, respectively, and are exothermic. Path **I.c** is not feasible because of the high barrier of 41.1 (36.1) kcal/mol. Later in the sequence of reactions, at complex **A15**, channel **I.b** may split into two new pathways leading to the same product **B8** with the Zr-$(\mu\text{-}\eta^2\text{-}NH)(\mu\text{-}H)(\mu\text{-}\eta^2\text{-}NH_2)Zr$ core. The first pathway, **A15** → **TS(A16)** → **A17** → **TS(B7)** → **B8**, proceeding via N−N bond cleavage leading to **A17** and then H_2 addition to give **B8**, is slightly more favorable than the second pathway of direct H_2 addition to **A15** to give **B8**. Thus, complex **A17**, $[p_2n_2]Zr(\mu\text{-}NH)_2Zr[p_2n_2]$, the thermodynamically most stable but kinetically not accessible product of the reaction of $[p_2n_2]Zr(\mu\text{-}\eta^2\text{-}N_2)Zr[p_2n_2]$, **A1**, with the first H_2, is now obtained with the aid of the second reacting hydrogen molecule.

4. Reaction of **B11** (**A3**) with H_2 occurs with a 21.3 kcal/mol barrier, via path **II.a** and leads to complex **B13** or **B13′**, where the N−H bonds are located cis to each other. Later, **B13** and **B13′**, which are isomers of the complex **B3**, rearrange to complex **B3** and can follow the path allowed for **B3**.

5. Present preliminary calculations suggest that addition of the third H_2 molecule to **A1** is kinetically less favorable than the first two.

Thus, the above presented findings and comparison of those with our previous results for the **A1** + H_2 reaction[6] and available experiments[4] indicate that addition of the second (and third) hydrogen molecule to complex $[p_2n_2]Zr(\mu\text{-}\eta^2\text{-}N_2)Zr[p_2n_2]$, **A1**, should be feasible under appropriate laboratory conditions. We encourage experimentalists to check our theoretical prediction.

Acknowledgment. The authors are grateful to Prof. Mike Fryzuk for simulating discussions. H.B. acknowledges the Visiting Fellowship from the Emerson Center. The present research is in part supported by a grant (CHE-9627775) from the National Science Foundation. Acknowledgment is also made for generous support of computing time at Bar Ilan University Computer Center, Emerson Center of Emory University, and U.S. National Center for Supercomputing Applications (NCSA).

Supporting Information Available: The optimized Cartesian coordinates of all reactants, transition states, and products of the reactions presented in this paper. This material is available free of charge via the Internet at http://pubs.acs.org.

OM000389Z